energies

Article

Development and Optimization of Chemical Kinetic Mechanisms for Ethanol–Gasoline Blends Using Genetic Algorithms

Filipe Cota [1,2,*], Clarissa Martins [1,2], Raphael Braga [1,2] and José Baeta [1,2]

[1] Graduate Program in Mechanical Engineering, Universidade Federal de Minas Gerais (PPGMEC-UFMG), Belo Horizonte CEP 31270-901, MG, Brazil; clarissammartins@ufmg.br (C.M.); raphaelmeireles@ufmg.br (R.B.); baeta@demec.ufmg.br (J.B.)
[2] Mobility Technology Center (CTM-UFMG), Department of Mechanical Engineering, Federal University of Minas Gerais, Antônio Carlos Avenue 6627, Belo Horizonte CEP 31270-901, MG, Brazil
* Correspondence: filipesc@ufmg.br

Abstract

Reduced chemical kinetic mechanisms are essential for enabling the use of complex fuels in 3D CFD combustion simulations. This study presents the development and optimization of a compact mechanism capable of accurately modeling ethanol–gasoline blends, including Brazilian Type-C gasoline (27% ethanol by volume) and up to pure ethanol (E100). An initial mechanism was constructed using the Directed Relation Graph with Error Propagation (DRGEP) method applied to detailed mechanisms selected for each surrogate component. The resulting mechanism was then refined through three global iterations of a genetic algorithm targeting ignition delay time (IDT) and laminar flame speed (LFS) performance. Five candidate versions (Mec1 to Mec5), each containing 179 species and 771 reactions, were generated. Mec4 was identified as the optimal configuration based on quantitative error analysis across all tested conditions and blend ratios. The final mechanism offers a balance between predictive accuracy and computational feasibility, making it well-suited for high-fidelity simulations in complex geometries involving multi-component ethanol–gasoline fuels.

Keywords: ethanol–gasoline surrogate; chemical kinetic mechanism; genetic algorithm optimization; mechanism reduction

check for updates

Academic Editor: Rocio Maceiras

Received: 25 June 2025
Revised: 13 July 2025
Accepted: 18 July 2025
Published: 21 August 2025

Citation: Cota, F.; Martins, C.; Braga, R.; Baeta, J. Development and Optimization of Chemical Kinetic Mechanisms for Ethanol–Gasoline Blends Using Genetic Algorithms. *Energies* **2025**, *18*, 4444. https://doi.org/10.3390/en18164444

Copyright: © 2025 by the authors. Licensee MDPI, Basel, Switzerland. This article is an open access article distributed under the terms and conditions of the Creative Commons Attribution (CC BY) license (https://creativecommons.org/licenses/by/4.0/).

1. Introduction

The global imperative to reduce greenhouse gas (GHG) emissions has intensified research into sustainable alternatives to conventional fossil fuels. Although electrification is progressing in Europe, the USA, and China, adoption strategies must consider regional contexts. In Brazil, the vast geography, predominant road transportation, and variable operational conditions present significant challenges to full electrification [1,2]. Consequently, ethanol—produced mainly from sugarcane—remains a key renewable option in the Brazilian energy matrix, providing both environmental and economic benefits [3].

The historical use of ethanol in Brazil dates to the early 20th century and gained traction with the "Pro-Álcool" program in the 1970s. The introduction of flex-fuel vehicles in 2003 significantly boosted ethanol demand, encouraging engine designs that fully exploit its high-octane rating and favorable combustion characteristics [3–6]. Compared to gasoline,

ethanol enables higher compression ratios, improves thermal efficiency, and reduces CO and HC emissions due to its oxygenated molecular structure and lower flame temperature [7,8].

Recent government initiatives, such as "Rota 2030" and the newly launched "Mover" program (Mobilidade Verde e Inovação, 2023), further reinforce ethanol's strategic role in decarbonizing Brazil's transportation sector. These policies stimulate R&D in cleaner combustion technologies, efficient engine calibration, and advanced fuel modeling [9–11].

Simulating the combustion of gasoline–ethanol blends, such as Brazilian Type-C gasoline (with 27% ethanol v/v), is complex due to the wide variety of hydrocarbons and oxygenates involved. These fuels can produce hundreds of intermediate species and thousands of elementary reactions during oxidation. While detailed chemical kinetic mechanisms offer high-fidelity modeling, they are computationally prohibitive in 3D CFD simulations [12,13]. This necessitates the development of reduced or skeletal mechanisms that strike a balance between accuracy and computational feasibility [14,15].

Several studies in recent years have addressed the challenge of balancing chemical accuracy with computational feasibility by developing reduced or skeletal kinetic mechanisms for gasoline, ethanol, or their blends. The foundational work by Marinov [16] remains a key reference for ethanol oxidation chemistry, providing a detailed mechanism widely used as a starting point for subsequent reductions. Likewise, the Computational Chemistry Consortium (C3) has contributed significantly to the development of highly detailed kinetic models for real fuel components, which, although not reduced themselves, serve as essential baselines for mechanism reduction and optimization efforts. Recent studies have applied advanced techniques such as DRGEP and directed sensitivity analysis to create compact yet accurate models. For example, Wang et al. [17] proposed a multipurpose skeletal core mechanism applicable across different thermodynamic conditions; Bellemans et al. [18] introduced an enhanced DRG-based reduction framework (P-DRGEP) suitable for high-performance combustion models; and Zhu et al. [19] constructed a skeletal multicomponent diesel surrogate mechanism using chemical lumping and genetic algorithms. These works reflect a growing effort toward achieving CFD-compatible mechanisms for complex fuel mixtures. The present study builds upon this foundation by creating and optimizing a mechanism capable of reproducing ignition and flame propagation behavior across the full range of ethanol–gasoline blends, with specific relevance to Brazilian fuel formulations.

In this work, a custom surrogate fuel was formulated based on a physicochemical analysis of a real E22 gasoline sample. To ensure representativeness, at least one chemical species was selected for each major hydrocarbon group found in gasoline—namely, paraffins, olefins, aromatics, and iso-paraffins—alongside ethanol as the oxygenated component [20,21]. A systematic evaluation of candidate mechanisms for each individual surrogate species was performed, using laminar flame speed (LFS) and ignition delay (IDT) as performance criteria. In cases where mechanisms were too large, the directed relation graph with error propagation (DRGEP) method was applied to reduce them without significant loss of fidelity [18,22]. The best-performing mechanism for each representative species was then merged into a composite mechanism, which served as the initial input for optimization.

To improve predictive performance across a wide range of operating conditions, the fused mechanism was then optimized using a genetic algorithm (GA). The optimization targeted the kinetic parameters of sensitive reactions and aimed to minimize errors in predicting IDT and LFS. This combined strategy of surrogate design, mechanism selection, reduction, fusion, and optimization aligns with best practices in recent literature for mechanism development [19–22].

2. Materials and Methods

The methodology proposed was divided into four steps, as described in Figure 1. The first one was the creation of a surrogate fuel composed of a smaller number of components than the complete ethanol/gasoline blend, based on physical chemistry analysis. The second step involved the evaluation of kinetic mechanisms available in the literature to represent each of the components defined in the surrogate fuel. In the following step, the selected individual mechanisms were reduced, when needed, based on the DRGEP approach, and combined to create the complete mechanism. In the fourth step, the mechanism was optimized based on a GA using IDT and LFS data.

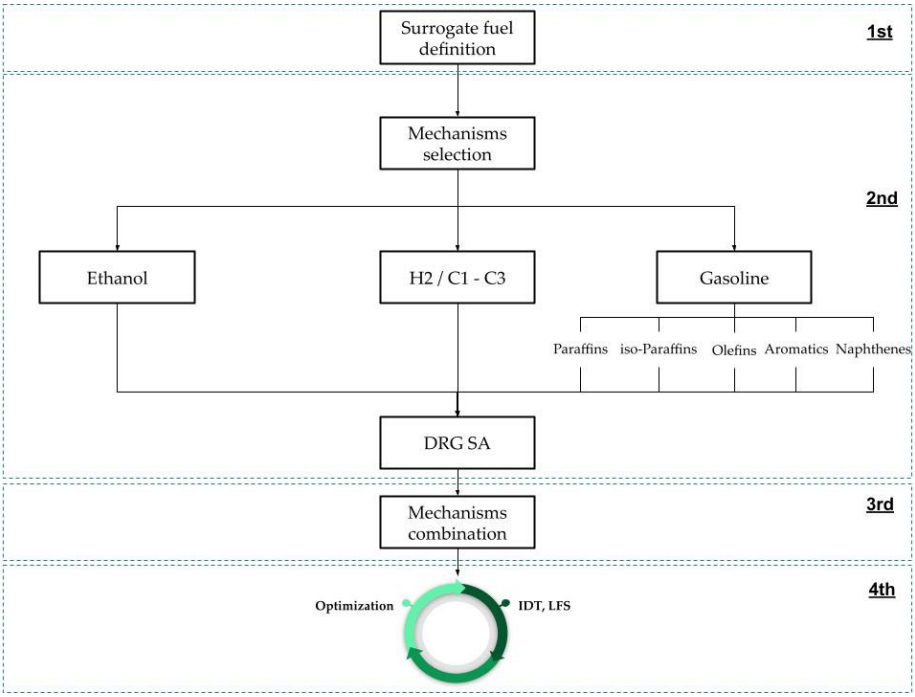


Figure 1. Workflow for the development and optimization of the chemical kinetic mechanism.

2.1. Surrogate Fuel Definition

For the surrogate definition, a physical–chemical characterization was conducted for the commercial Brazilian gasoline type C by the Fuel Testing Laboratory of the Chemical Department at the Federal University of Minas Gerais (UFMG), Belo Horizonte CEP 31270-901, MG, Brazil. The parameters used included detailed hydrocarbon analysis (DHA/PIANO/PONA), ethanol content (PROVETA–NBR 13992 [23]), higher and lower heating values (ASTM D4809-18 and D240 [24,25]), H/C and O/C ratios, and MON (ASTM D2700 [26]), RON (ASTM D2699 [27]).

The detailed hydrocarbon analysis was used as a reference to define species to represent the main fuel groups: iso-paraffins, n-paraffins, olefins, aromatics, naphthenes, and ethanol. Based on that, considering together the availability of chemical kinetic mechanisms in the literature, the surrogate components were defined.

To define the best ratio between the components to match the actual fuel properties, a MATLAB R2024a, (The MathWorks, Inc., Natick, MA, USA) script was created to vary the species molar fractions until the surrogate properties became close to the experimental data, just fixing the ethanol content that was already directly measured.

The script considers that the properties of the fuel are a function of its components' properties, balanced by their respective molar fractions according to Equation (1).

$$\Phi_s = \sum_i \Phi_i x_i, \quad (1)$$

where Φ_s is any property of the mixture, Φ_i is the same property for species i, and x_i is the molar fraction of species i. The optimization process is carried out such that the objective function, f, is minimized according to Equation (2).

$$f = \sum_j w_j R_j^2, \quad (2)$$

where w_j is the weight assigned to property j, ranging from 0 to 1, and R_j is the error defined by Equation (3).

$$R_j = T_j - \sum_j \Phi_{ij} x_i, \quad (3)$$

To define the composition of the remaining gasoline and ethanol blends, ranging from 27% to 100% ethanol by volume, the first step was to determine the fraction of components present in sample *E*27 that corresponds solely to gasoline, excluding the ethanol fraction. This yields the composition of the *E0* blend (0% ethanol). To achieve this, the ethanol fraction of *E*27 was removed, and the fractions of the remaining species were redistributed according to Equations (4) and (5).

$$V_{E27_gas} = V_{E27_total} - V_{E27_Ethanol}, \quad (4)$$

$$v_{E0_j} = \frac{v_{E27_j}}{V_{E27_gas}}, \quad (5)$$

where V_{E27_gas} is the volume corresponding to the gasoline fraction in fuel *E27*, excluding the volume of ethanol ($V_{E27_Ethanol}$), v_{E0_j} is the volumetric fraction of species *j* in fuel *E*0, and v_{E27_j} is the volumetric fraction of species *j* in the sample of type C gasoline. It is emphasized that j represents only the species corresponding to the gasoline fraction in the fuel, not including ethanol. Based on the composition of fuel *E*0, any other blends were prepared by adding the desired volume of ethanol, redistributing the corresponding fraction of each species according to Equations (6) to (8).

$$V_{Ex_total} = V_{E0_gas} + V_{Ex_Ethanol}, \quad (6)$$

$$v_{Ethanol} = \frac{V_{Ex_Ethanol}}{100}, \quad (7)$$

$$v_{Ex_j} = v_{E0_j} * V_{Ex_gas}, \quad (8)$$

where $V_{Ex_Ethanol}$ is the total volume of blend *Ex* (*E*0–*E*100). $V_{Ex_Ethanol}$ and V_{Ex_gas} are the volumes of ethanol and gasoline corresponding to fuel *Ex*, respectively. The volumetric fraction of ethanol is given by $v_{Ethanol}$, and v_{Ex_j} is the volumetric fraction of species *j* in fuel *Ex*.

2.2. Individual Mechanisms Selection

Six species were selected to represent the fuel groups: iso-paraffins, n-paraffins, olefins, aromatics, naphthenes, and ethanol. One mechanism was selected for each species and evaluated with IDT and LFS data. Additional mechanisms for H_2 and C_0–C_3 species were also included. Some mechanisms available in the literature are not specifically built for individual species but for mixtures. Others are individual mechanisms; however, they are too detailed to effectively represent their respective fuels, often making them impractical for 3D simulations. Therefore, in both cases, it is necessary to reduce these mechanisms to make them species-specific and of a size that still allows their use in more complex simulations. Thus, when required, mechanisms selected for individual species underwent an extraction or reduction process for each component using the Direct Relation Graph with Error Propagation (DRGEP) method using the Chemistry tool of the software

CONVERGE v3.1 (Convergent Science, Inc., Madison, WI, USA), thereby generating a species-specific skeletal mechanism. Figure 2 includes the flow chart applied during the reduction/extraction process.

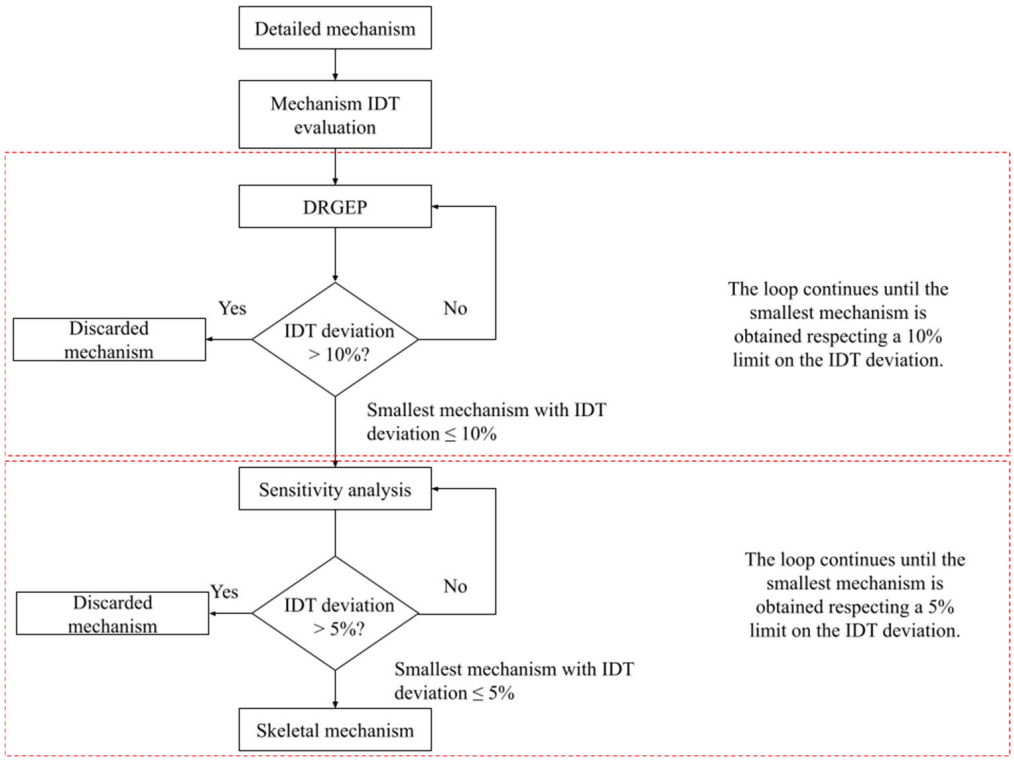


Figure 2. Workflow of the reduction/extraction of skeletal mechanism from detailed ones.

The selection of the mechanism representing each species of the surrogate fuel was based on two criteria: the relative error, considering experimental data, and the total computation time required for IDT and LFS simulations of each species using each candidate mechanism. To this end, a fixed set of conditions for pressure, temperature, and equivalence ratio was defined for both IDT and LFS simulations, based on the availability of experimental data for each species reported in the literature. At the end of the analysis, the mechanisms were ranked in ascending order according to the normalized mean square error (*nMSE*), relative to the mechanism with the largest deviation, and by the total processing time required to simulate all conditions. All simulations were carried out on the same server using 56 cores to ensure comparability of simulation times across mechanisms. The final mechanism selection aimed to balance result accuracy and computational cost.

Mechanism Reduction/Extraction

The concept of creating a skeletal kinetic mechanism consists of identifying and removing unimportant chemical species and the elementary reactions associated with them from a complete mechanism.

The DRGEP method uses a digraph representation, as shown in Figure 3, of the complete kinetic mechanism composed of vertices connected by edges with specific directions. Each vertex represents a species in an elementary reaction of the mechanism; an edge exists between two vertices if the two species represented by them are present in the same reaction.

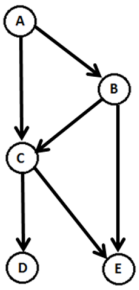


Figure 3. Schematic configuration of the DRGEP, © Convergent Science, Inc. All rights reserved. Used with permission [28].

The DRG method starts by coupling directly related species present in the same reaction, which implies that the removal of species *B* from the mechanism described in Figure 3 leads to an error in the production rate of species *A*. This error, r_{AB}, can be obtained from Equation (9).

$$r_{AB} \equiv \frac{\sum_{i=1,I} |v_{A,i}\omega_i\delta_{Bi}|}{\sum_{i=1,\ I} |v_{A,i}\omega_i|}, \tag{9}$$

$$\delta_{Bi} = \begin{cases} 1, \ if\ the\ i^{th}\ reaction\ involves\ species \\ B\ 0, \ any\ other\ way, \end{cases}$$

where $v_{A,i}$ indicates the stoichiometric coefficient of species *A* in a reaction *i*; ω_i is the difference between the forward and backward reactions in net rates. The terms in the denominator of Equation (9) represent the contributions of each reaction to the rate of production of species *A*. The terms in the numerator correspond to the influence of the reactions that contain the species *A* and *B*.

The analysis starts with a set of major species, the fuel species, for example. Each major species will have a digraph as shown in Figure 3. The final mechanism will be a combination of all major species digraphs.

If the error, r_{AB}, overcomes a defined threshold value, ε (cut-off tolerance), the elimination of species *B* would lead to a considerable error in the rate of production of *A*; therefore, species *B* must be retained on the skeletal mechanism. There are also species that are indirectly connected to the major ones. That is the case of species *D* and *E* presented in Figure 3. Species *D* and E are indirectly connected to species *A* by intermediate species *C* and *B*, respectively. The indirectly connected species are maintained in the final mechanism if they are required for the correct prediction of the production rate of the intermediate species between them and the major species.

During the reduction process, the software CONVERGE calculates all r_{AB} coefficients and then, different values of ε are imposed, and a reduced mechanism is generated for each one of them. One by one, all reduced mechanisms are used to create an IDT profile, and then, the data obtained is compared with the one from the detailed mechanism. The optimum mechanism is chosen as the smallest one with an IDT deviation from the obtained using the detailed mechanism lower than the tolerance defined by the user.

2.3. Mechanism Optimization Using Genetic Algorithm

The method defined for the optimization of the mechanism was the GA optimization. This method mimics the biological principle of evolution to optimize models. Again, the software used was the CONVERGE CFD 3.1v through its optimization tool, named CONGO.

According to the structure of the GA of optimization, some elements need to be defined. The first is the individuals who are defined by the set of information that will be varied to achieve the desired optimization. In this work, individuals are defined as each

version of the mechanism that was randomly generated at first and has the potential to be considered as an optimal mechanism.

The information that defines an individual is called genes, and it is the information chosen to characterize an individual and is also the points that will vary throughout the implementation of the algorithm. The parameter chosen as the gene is the pre-exponential factor (A_r) of the modified Arrhenius law. This factor defines the fraction of collisions between molecules of a chemical reaction capable of doing an atomic reconfiguration that leads to the formation of products.

The parameter A_r is presented in each of the chemical reactions that make up a kinetic mechanism. Hence, the number of genes set during the GA implementation is the number of reactions that will have their A_r parameters changed to optimize the mechanism.

Another important term is population size, which is defined as a set of individuals with the potential to be an optimal solution for the model. The maximum number of generations defines the number of iterations conducted to reach the correlation factor. Therefore, even if the target is not matched, the algorithm would not be run for an undefined period. A mutation factor is included in the algorithm to reduce the chances of reaching a local maximum optimization condition.

During the optimization process, initially, a random population is created, and its individuals are subjected to an assessment to see how well adapted each of them is to the desired condition. This assessment is made through a mathematical function defined as a fitness function. This function is modeled in such a way that the most adapted individuals are "rewarded", and the least adapted individuals are "punished".

For the optimization of kinetic mechanisms, the fitness function is defined as the deviation from a target value, which is the optimal value for each IDT and LFS simulation condition, as shown in Equation (10).

$$f_{Merit} = \sum_{n_{Tg}} 1 - \left| \frac{ig_{calc} - ig_{target}}{ig_{target}} \right| \tag{10}$$

where n_{Tg} is the number of targets defined, ig_{calc} is the simulated result, and ig_{target} is the experimental value defined as the target. Hence, according to Equation (10), for each point when the calculated value is closer to the target, the result of the equation is close to 1, as the equation is the summation of each point, the mechanism is more adapted when its fitness function presents a result closer to the number of experimental targets, n_{Tg}.

After the individuals are ordered according to the values obtained by each mechanism through the fitness function, the formation of the next generation begins. This generation is obtained by crossing the genes of the best individuals in a process defined as cross-over and through mutations. Mutation is responsible for changing the values of some genes of the individual to add variety within the population, and may even add new characteristics to an individual, making it better than the initial ones. This process helps to avoid obtaining local maxima, which would undermine the final solution obtained.

The steps described are repeated until the finishing criteria are reached, as summarized in Figure 4.

The parameters defined for the GA optimization in this project are presented in Table 1.

As shown in Table 1, the criteria defined for the completion of the optimization simulation are the maximum number of generations and the correlation factor. In this study, four iterations of the genetic algorithm (GA) were conducted. Each iteration employed the same set of parameters described in Table 1, with the initial mechanism for each iteration corresponding to the optimized result obtained from the previous one.

Table 1. Genetic algorithm parameters.

Parameters	Value
Population size	10
Number of genes	20
Mutation factor	0.2
Maximum number of generations	1000
Correlation factor	0.95

During the optimization algorithm application, a weighting factor of 1.0 was assigned to LFS targets and 0.7 to IDT targets. This strategy was adopted to favor mechanisms that more accurately capture flame propagation behavior. The choice was motivated by the intended application of the mechanism in 3D CFD simulations, where accurate flame propagation modeling is of primary importance. In addition, experimental datasets for LFS were more consistently available across the range of ethanol–gasoline blends considered, allowing for a more uniform optimization process. While no formal sensitivity study of the weighting parameters was conducted, this configuration was found to provide a practical balance between the two performance metrics and led to consistent improvements during the iterative optimization process, enhancing LFS prediction without compromising the accuracy of IDT results.

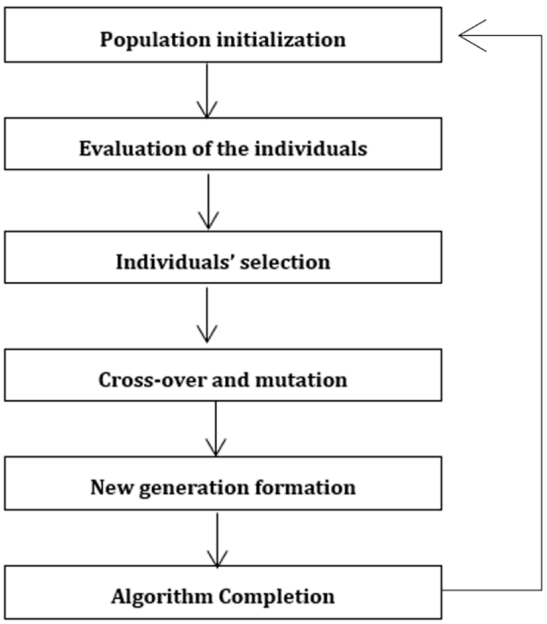


Figure 4. Schematic structure of the genetic algorithm of optimization.

3. Results

3.1. Surrogate Definition

The selection of species to represent the surrogate fuel components was guided by a comprehensive chemical analysis of the E27 fuel sample, the surrogate's ability to reproduce the chemical behavior of the real fuel, and the availability of detailed chemical kinetic mechanisms for each candidate species. Table 2 presents the final volumetric percentage for each species in the E27 surrogate fuel obtained through the optimization script developed in MATLAB.

Table 2. Fuel surrogate and experimental composition.

Experiment		Surrogate	
Group	*v*/*v*%	Species	*v*/*v*%
Aromatics	16.00	Toluene	12.5
iso-paraffins	30.50	iso-octane	20.58
Naphthenes	13.53	MCH	11.38
Olefins	4.50	1-hexene	13.72
n-paraffins	8.74	n-heptane	15.07
Ethanol	26.73	Ethanol	26.75

Although 1-hexene and n-heptane were not the most abundant compounds within the olefinic and n-paraffinic classes, respectively, they were selected because these compounds have been extensively studied by major research laboratories in the field, and numerous authors have published kinetic mechanisms for their representation. The final surrogate composition also included iso-octane, toluene, methyl-cyclohexane (MCH), and ethanol, representing iso-paraffins, aromatics, naphthenes, and ethanol itself, respectively.

According to the composition presented in Table 2, Figure 5 provides the surrogate properties normalized by the experimental results; the closer the result is to one, the better the property is represented by the surrogate fuel proposed.

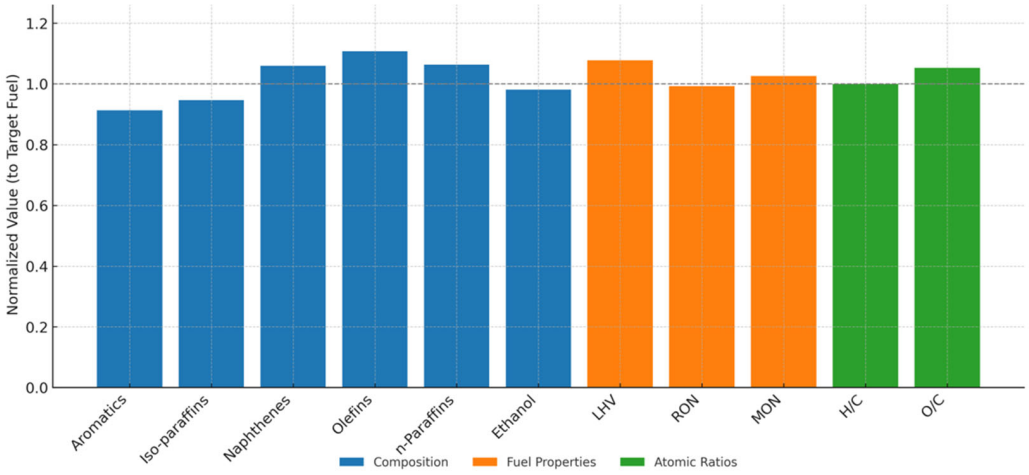


Figure 5. Normalized surrogate fuel properties by category.

According to the results shown in Figure 5, the surrogate fuel showed good agreement across most of the properties evaluated, with deviations below 10% in all categories. These results demonstrate that the surrogate formulation captures both structural and energetic attributes of the real fuel, supporting its applicability in chemical kinetic modeling and combustion simulations.

3.2. Individual Mechanism Selection

Several mechanisms were tested for each component of the fuel surrogate, as represented in Table 3.

Table 3. Chemical kinetic mechanism for the individual fuel components.

Component	Mechanism	Species	Reactions	Reference
Ethanol	Marinov et al. (1999)	57	383	[16]
	Mittal et al. (2014)	113	710	[29]
	Roy et al. (2020)	67	1016	[8]
	C3 (2022)	3761	16,522	[30]
	Shi et al. (2021)	76	280	[31]
	Merino et al. (2018)	34	69	[32]
1-Hexene	C3 (2022)	3761	16,522	[30]
	Lei Zhang et al. (2021)	145	653	[33]
	LLNL (2011)	1393	5969	[34]
	Ranzi et al. (2014)	339	9781	[35]
	Yang et al. (2021)	97	308	[36]
isoOctane	C3 (2022)	3761	16,522	[30]
	Lei Zhang et al. (2021)	145	653	[33]
	LLNL (2011)	1393	5969	[34]
	Liu et al. (2013)	56	168	[37]
	Ranzi et al. (2014)	339	9781	[35]
	Tsurushima et al. (2009)	33	38	[38]
	Cota (2018)	75	331	[39]
MCH	LLNL (2011)	1393	5969	[34]
	Krithika et al. (2015)	3761	16,522	[40]
	Ranzi et al. (2012)	492	17,790	[41]
	Tong Yao et al. (2017)	70	377	[42]
	Liu et al. (2013)	56	168	[37]
	Stagni et al. (2016)	201	4417	[43]
Toluene	Liu et al. (2013)	56	168	[37]
	C3 (2022)	3761	16,522	[30]
	Chang et al. (2015)	70	220	[44]
	Cota (2018)	75	331	[39]
	Cai e Pitsch (2015)	339	2791	[45]
n Heptane	C3 (2022)	3761	16,522	[30]
	Lei Zhang et al. (2021)	145	653	[33]
	LLNL (2011)	1393	5969	[34]
	Liu et al. (2013)	56	168	[37]
	Ranzi et al. (2014)	339	9781	[35]
	Cota (2018)	75	331	[39]
	Tsurushima et al. (2009)	33	38	[38]

To enable the application of detailed chemical kinetic models in 3D CFD simulations, a substantial reduction in mechanism size was required. The original C3 mechanism [30] and LLNL [33] are computationally prohibitive for 3D CFD simulations, considering the computational resources available for this study. Therefore, both mechanisms were reduced using the approach detailed in Section Mechanism Reduction/Extraction, obtaining lighter versions better suited for numerical implementation. The reduced C3_Red mechanism contained 300 species and 1085 reactions, and the reduced LLNL_Red version consisted of 280 species and 1342 reactions.

The mechanisms for each species were tested in different conditions for pressure, temperature, and equivalence ratio, as represented in Table 4.

Table 4. Individual species correlation conditions.

	IDT			LFS		
Species	**P [bar]**	**T [K]**	**phi**	**P [bar]**	**T [K]**	**phi**
Ethanol	10–50	750–1300	1.0	1; 2; 7; 10	298–428	0.6–1.8
Toluene	16–50	900–1450	0.25; 0.5; 1.0	1; 5	298–358	0.6–1.6
1-Hexene	10–30	650–1250	1.0	1.0; 10	373	0.6–1.5
Iso-Octane	10–40	625–1450	0.5; 1.0; 2.0	1.0; 5; 10	298–470	0.6–1.4
MCH	12–50	650–1250	1.0	1.0; 5; 10	353	0.6–1.6
n-Heptane	13–43	550–1450	0.25; 0.5; 1.0	1.0; 2.5; 5.0	328–600	0.6–1.6

To facilitate the comparison between the chemical kinetic mechanisms for each species, bar charts were created for IDT and LFS—Figures 6 and 7, respectively—with two metrics: nMSE and normalized computational time. The species are represented by different colors, where the darker bar indicates the normalized error and the lighter bar of the same color represents the normalized simulation time.

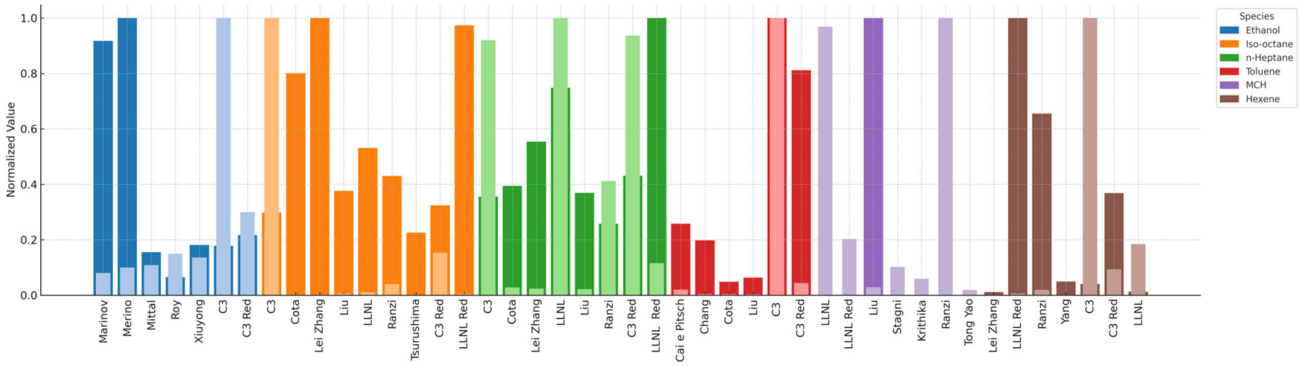


Figure 6. Normalized mean square error and normalized simulation time for each species and kinetic mechanism tested for IDT.

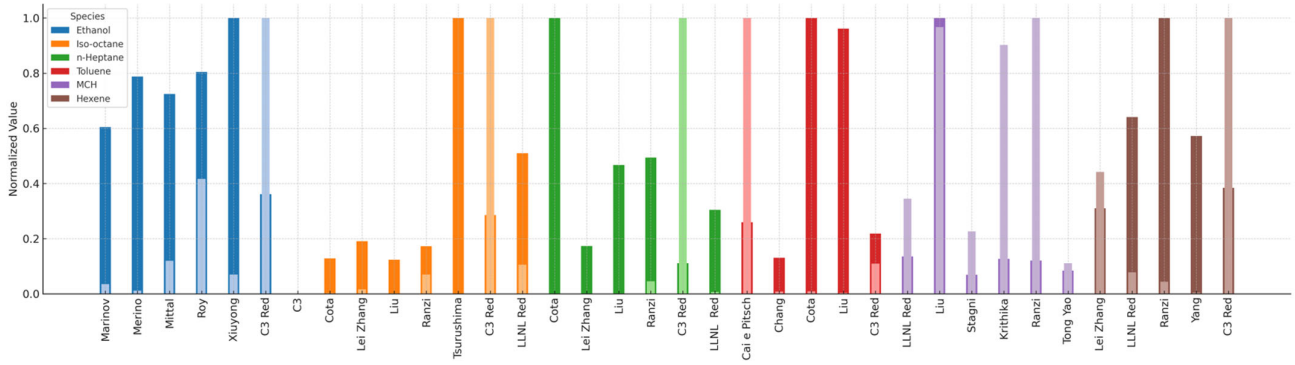


Figure 7. Normalized mean square error and normalized simulation time for each species and kinetic mechanism tested for LFS.

For iso-octane, the mechanism by Liu et al. [37] showed the most balanced performance, with low nMSE in both IDT and LFS and reduced computational time compared to larger mechanisms like LLNL_Red [30] or C3_Red [30]. Notably, Tsurushima's mechanism [38] offered good accuracy in IDT but exhibited a higher error in LFS, making it less robust across all conditions.

Regarding n-heptane, Liu et al. [37] again provided consistent results with moderate simulation time and acceptable accuracy. Although the C3_Red mechanism [30] had the lowest error in LFS, it required significantly higher computational time, which reduced its practicality for future CFD integration.

For toluene, Chang et al.'s mechanism [44] offered a good compromise, with solid accuracy in both IDT and LFS and the shortest total simulation time. While Liu et al. [37] and Cota [39] mechanisms showed superior IDT accuracy, they were either less consistent in LFS or more computationally demanding.

In the case of 1-hexene, the Yang et al. mechanism [36] showed the greatest compromise between accuracy and simulation time. The mechanism from Lei Zhang [33] showed the lowest total error, but its simulation time is almost 100 times that of Yang's simulation time. The Ranzi [35] and LLNL [34] reduced mechanisms exhibited considerably higher errors in both metrics.

For MCH, the mechanism proposed by Tong Yao [42] achieved a strong balance—low error in LFS and IDT with a relatively compact structure, outperforming more detailed mechanisms, such as Ranzi [41] or LLNL [34] in computational efficiency.

Finally, for ethanol, the mechanism developed by Mittal [29] delivered the best overall performance in IDT, along with competitive LFS accuracy, justifying its selection despite its slightly higher size. The mechanism by Roy [8], although highly accurate in IDT, showed higher computational cost and nMSE for LFS simulations.

It is important to emphasize that the process of merging mechanisms is not a simple summation of species and reactions, because many species are shared among the individual mechanisms. As a result, the number of species and reactions of the global mechanism—Mec01—are, respectively, 179 and 771.

3.3. Mechanism Optimization

The mechanisms for ethanol/gasoline mixtures were tested under a wide range of conditions of pressure, temperature, and equivalence ratio, as summarized in Table 5.

Table 5. Global mechanism correlation conditions.

	IDT			LFS		
Mixture	**P [bar]**	**T [K]**	**phi**	**P [bar]**	**T [K]**	**phi**
E0	25–55	650–1450	1.0	1.0; 2.5	373	0.6–1.4
E22	12–50	650–1250	0.25; 0.5; 1.0	1.0	360	0.6–1.2
E40	10–50	750–1250	1.0	-	-	-
E50	25	750–1150	0.5	1.0	360; 480	0.6–1.4
E85	25	750–1100	0.5	1.0	353	0.6–1.6
E100	10–50	750–1250	1.0	1.0–7.0	298–420	0.6–1.6

Due to the extensive volume of simulation data, not all results are presented in this work. Instead, a representative subset was selected to illustrate the overall performance trends. Four fuel blends were chosen (E22, E50, E85, and E100), and for each blend, one plot of IDT and one of LFS, Figures 8 and 9, are included to provide a clear assessment of the predictive mechanisms' capabilities under different operating regimes. The remaining plots for all tested blends and different conditions are available in Supplementary Materials—Figures S1–S12.

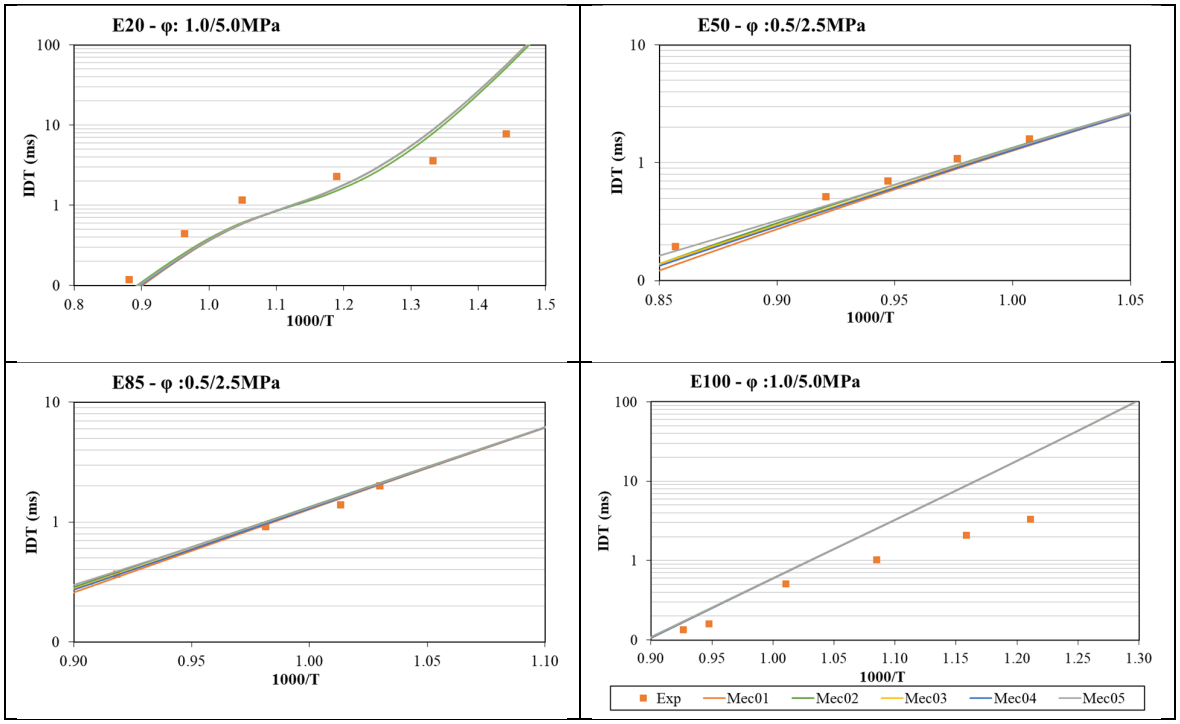


Figure 8. Global mechanisms IDT comparison—Optimization iterations. Exp.: E22 [46]; E50, E85 [47]; E100 [48].

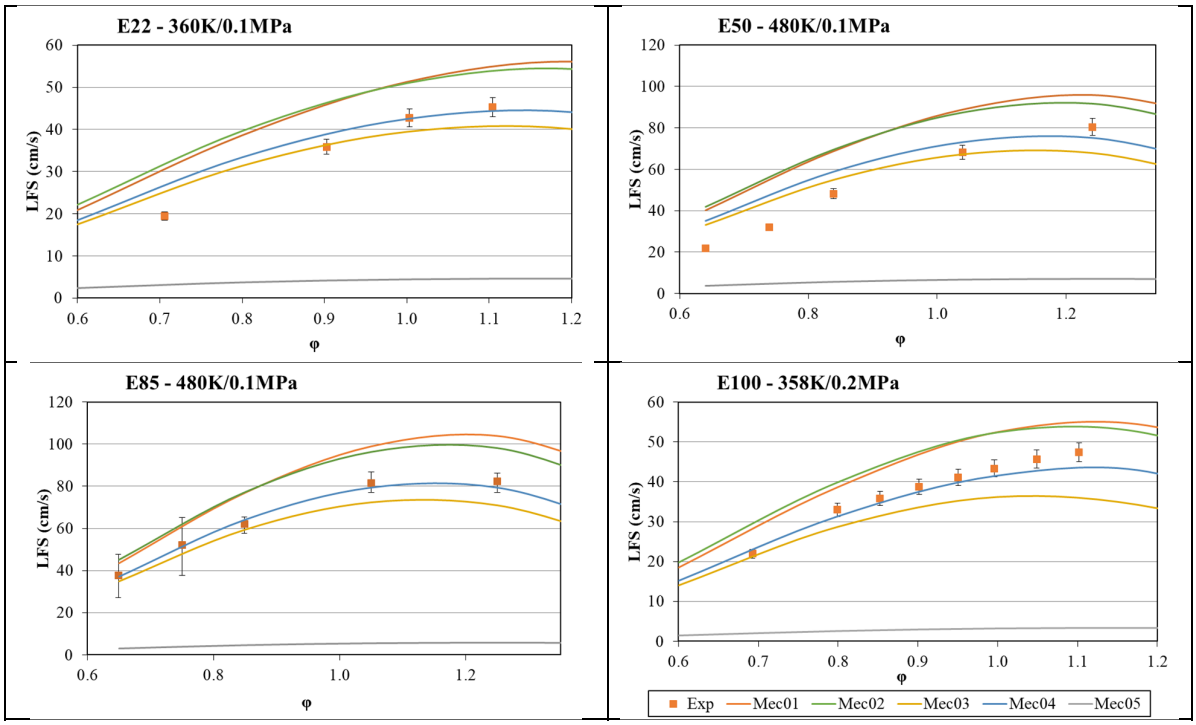


Figure 9. Global mechanisms LFS comparison—Optimization iterations. Exp.: E22, E50, E85 [39]; E100 [8].

Figure 8 presents the IDT predictions for selected ethanol–gasoline blends for different thermodynamic conditions. For all tested mixtures, the five evaluated mechanisms exhibited relatively small differences among themselves. Despite the limited variation between models, all mechanisms were able to reasonably reproduce the trends observed in experimental data, especially in the intermediate and high-temperature regimes. This

consistent behavior across mechanisms suggests that the optimization process led to a convergence in predictive performance.

The reduced sensitivity between mechanisms may be partially attributed to the lower weighting factor assigned to IDT in the optimization algorithm compared to LFS. This configuration favored the selection of mechanisms that perform well in flame propagation simulations, which was the main objective of the study. Nonetheless, even with a lower optimization priority, the mechanisms demonstrated robust performance in capturing the ignition characteristics of ethanol–gasoline blends, confirming their suitability for further application in engine combustion modeling.

Figure 9 illustrates the LFS predictions for selected ethanol–gasoline blends. A clear trend is observed throughout the optimization process: the results become progressively closer to the experimental data up to the third iteration (Mec4), indicating that the optimization algorithm was successful in calibrating the kinetic parameters with respect to flame propagation.

However, in the final iteration, the model produced Mec5, which exhibited a very different behavior, losing the ability to accurately capture the flame speed profile across all blends and equivalence ratios.

4. Discussion

Starting from the base mechanism (Mec1), four successive iterations of the optimization process were carried out, resulting in mechanisms Mec2 through Mec5. As evidenced by the nMSE—Figures 10 and 11—this iterative strategy produced a clear enhancement in model performance, especially with respect to LFS, particularly during the first three iterations. The differences between the results for each mechanism for IDT were less significant, as already discussed.

For LFS, Mec3 yielded significantly lower nMSE values than Mec2 and produced the best results for several fuel mixtures. Mec4 sustained this tendency, demonstrating a performance comparable to Mec3 while providing more consistent results across all tested ethanol–gasoline mixtures.

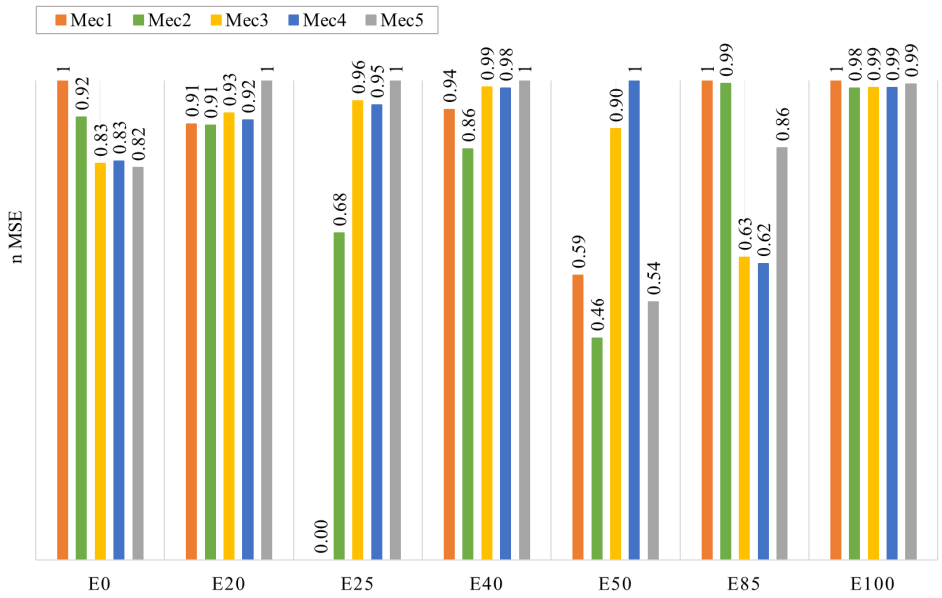


Figure 10. Normalized MSE for Mec1, Mec2, Mec3, Mec4 and Mec5 for IDT.

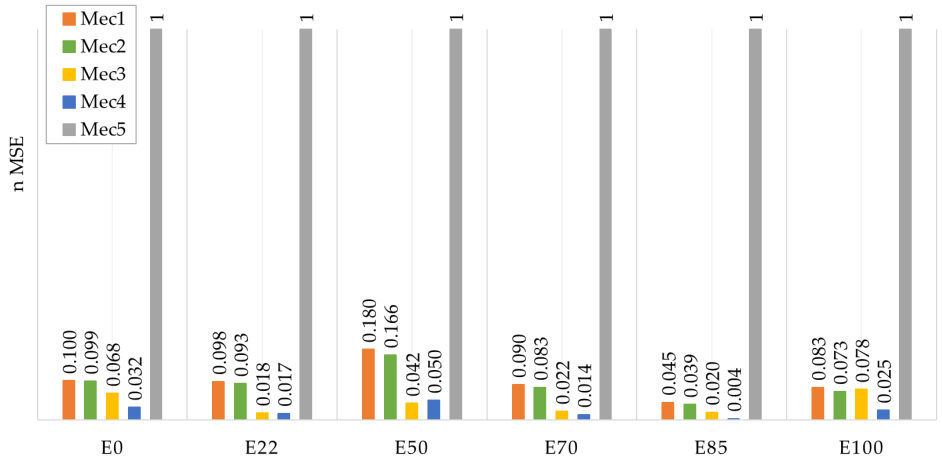


Figure 11. Normalized MSE for Mec1, Mec2, Mec3, Mec4 and Mec5 for LFS.

A different behavior was observed in the final iteration. Although Mec5 maintained satisfactory predictive accuracy for IDT, it exhibited the maximum nMSE for LFS across all mixtures, indicating a complete loss of predictive capability for this property. Moreover, the model was unable to replicate the typical parabolic shape of the LFS curve with respect to equivalence ratio, a well-established behavior for both hydrocarbon and oxygenated fuel combustion, extensively documented in the literature [17,49] as can be seen with the application of widely validated and disseminated mechanisms in the literature, such as GRI-Mech 3.0 [50], Marinov's mechanism [16], and the C3 mechanism [30]. A plausible hypothesis for the poor performance of Mec5, particularly in predicting LFS, is that the genetic algorithm may have excessively modified the kinetic parameters of reactions crucial to radical propagation pathways. These include chain-branching and chain-propagating reactions involving highly reactive species such as H, OH, and HO_2. Given that flame speed is strongly dependent on the equivalence ratio, such alterations could have disrupted the balance of reaction pathways across different φ values. This would explain the observed deviation from the typical parabolic trend in LFS results for Mec5. The observed loss of generalization suggests an overfitting to a limited set of conditions during the final optimization step [51,52].

Therefore, when considering the combined performance of the mechanisms in terms of both IDT and LFS, as well as the stability of results across the different mixture compositions, Mec4 is identified as the most suitable. This selection was based on a multi-objective evaluation, which simultaneously considered the normalized mean square error for both combustion properties. Among all the versions tested, Mec4 provided the lowest overall deviation while maintaining consistent predictive behavior across blends and operating conditions. It offers a robust balance between accuracy in ignition prediction and fidelity in flame propagation modeling, thus justifying its selection as the representative kinetic mechanism for the ethanol–gasoline combustion simulations conducted in this study.

Future research will focus on implementing and validating Mec4 in 3D engine simulations, assessing its performance in terms of in-cylinder pressure, flame front propagation, and pollutant formation. These studies will provide a comprehensive evaluation of the mechanism's predictive capabilities in complex geometries and transient operating regimes. The insights gained from these applications will support the refinement of surrogate formulations and optimization workflows, reinforcing the use of reduced kinetic mechanisms as practical tools in engine design and emission control.

5. Conclusions

A surrogate fuel composed of the following six species was created based on experimental characterization of a Brazilian gasoline type C sample: iso-octane; n-heptane; toluene; methyl cyclohexane; 1-hexene; ethanol. The chemical kinetic mechanism created was validated based on ignition delay time and laminar flame speed simulations.

1- The corresponding v/v% for each species was: 12.5%, 20.58%, 11.38%, 13.72%, 15.07%, 26.75% for toluene, iso-octane, methyl cyclohexane, 1-hexene, n-heptane, and ethanol, respectively. This surrogate presented a good correlation with experimental data of organic groups composition, lower heating value, research octane number, motor octane number, H/C, and O/C.
2- Several mechanisms were tested for the individual species and compared with experimental data of ignition delay time and laminar flame speed. A square mean error analysis, together with simulation time, was used to select one mechanism for each species.
3- The mechanisms from LLNL [34] and C3mech [30] were reduced before the evaluation through the directed relation graph with error propagation method, with a reduction of 92% for species and 93% for reactions, and 79% for species and 77% for reactions, respectively.
4- The mechanisms chosen for each species were: Toluene [44], iso-octane [37], methyl cyclohexane [42], 1-hexene [36], n-heptane [37], and ethanol [29]. The global mechanism (Mec1) was composed of 179 species and 771 reactions.
5- The global mechanism was optimized, starting with Mec1, in four iterations of a genetic algorithm using ignition delay time and laminar flame speed experimental data as targets, with a weight factor of 0.7 for ignition delay time and 1.0 for laminar flame speed. A clear improvement in each iteration was observed until Mec4 was created. After that, the final iteration created Mec5, which lost its capability to represent laminar flame speed data, even though the results for ignition delay time were comparable to the previous versions of the mechanism.

The methodology used in this study was successfully implemented, and an optimized mechanism (Mec4) was validated for gasoline/ethanol mixture in a wide range of concentrations while keeping a relatively small size, showing a great potential for its application in 3D CFD simulations of complex systems such as internal combustion engines.

Supplementary Materials: The following supporting information can be downloaded at: https://www.mdpi.com/article/10.3390/en18164444/s1. Figures S1–S12: Ignition delay time and Laminar flame speed simulations for the global mechanism validation.

Author Contributions: F.C.: Conceptualization, Methodology, Investigation, Formal analysis, Writing—original draft. C.M. and R.B.: Writing—review and editing. J.B.: Supervision, Review, Funding acquisition. All authors have read and agreed to the published version of the manuscript.

Funding: This study was financed in part by the Coordenação de Aperfeiçoamento de Pessoal de Nível Superior—Brasil (CAPES)—Finance Code 001.

Data Availability Statement: Data will be made available on request.

Acknowledgments: The authors would like to thank the "programa de pós graduação—PPGMEC" of UFMG's mechanical engineering graduate program. The authors would also like to thank CAPES for accessing the journal portal "Periódicos CAPES". Finally, the authors would like to thank the CONVERGE CFD team for providing the software licenses and for the dedicated technical support provided.

Conflicts of Interest: The authors declare that they have no known competing financial interests or personal relationships that could have appeared to influence the work reported in this paper.

Abbreviations

The following abbreviations are used in this manuscript:

CFD	Computational Fluid Dynamics
DHA	Detailed Hydrocarbon Analysis
DRGEP	Directed Relation Graph with Error Propagation
E0–E100	Ethanol–Gasoline Blends 0% to 100% Ethanol by Volume
GA	Genetic Algorithm
GHG	Greenhouse Gases
HCCI	Homogeneous Charge Compression Ignition
H/C	Hydrogen-to-Carbon Ratio
IDT	Ignition Delay Time
LFS	Laminar Flame Speed
LHV	Lower Heating Value
LLNL	Lawrence Livermore National Laboratory
MCH	Methylcyclohexane
MON	Motor Octane Number
nMSE	Normalized Mean Square Error
O/C	Oxygen-to-Carbon Ratio
PRF	Primary Reference Fuel
RON	Research Octane Number

References

1. Glyniadakis, S.; Balestieri, J.A.P. Brazilian light vehicle fleet decarbonization scenarios for 2050. *Energy Policy* **2023**, *181*, 113682. [CrossRef]
2. Pacheco, A.F. Analysis and Reduction of Detailed Chemical Kinetics Mechanisms for Combustion of Ethanol and Air. Dissertação de Mestrado, Universidade Federal de Santa Catarina, Centro Tecnológico, Florianópolis, Santa Catarina, Brazil, 2016.
3. Santos, N.D.S.A.; Roso, V.R.; Malaquias, A.C.T.; Baeta, J.G.C. Internal combustion engines and biofuels: Examining why this robust combination should not be ignored for future sustainable transportation. *Renew. Sustain. Energy Rev.* **2021**, *148*, 111292. [CrossRef]
4. Eaglin, J. The History of Ethanol Production in Brazil with a Focus on Environmental Health. In *Oxford Research Encyclopedia of Latin American History*; Oxford University Press: Oxford, UK, 2024.
5. Aguiar, D.R.D.; Taheripour, F.; Silva, D.A.L. Ethanol fuel in Brazil: Policies and carbon emission avoidance. *Biofuels* **2025**, *16*, 248–258. [CrossRef]
6. Stolf, R.; de Oliveira, A.P.R. The success of the Brazilian alcohol program (PROÁLCOOL)-a decade-by-decade brief history of ethanol in Brazil. *Eng. Agrícola* **2020**, *40*, 243–248. [CrossRef]
7. Malaquias, A.C.T.; de Paula Araújo, G.H.; Amaral, L.V.; de Carvalho Torres Filho, M.; Chavda, N.B.; Pujatti, F.J.P.; Baêta, J.G.C. Experimental characterization of ethanol controlled auto-ignition in a single-cylinder research engine. *Case Stud. Therm. Eng.* **2025**, *70*, 106128. [CrossRef]
8. Roy, S.; Askari, O. A New Detailed Ethanol Kinetic Mechanism at Engine-Relevant Conditions. *Energy Fuels* **2020**, *34*, 3691–3708. [CrossRef]
9. Cieplinski, A. *O Potencial de Descarbonização do Programa MOVER: Explorando Variações nas Vendas de Veículos de Diferentes Tecnologias até 2027*; International Council on Clean Transportation (ICCT): Brasília, Brasil, 2024. Available online: https://theicct.org/publication/o-potencial-de-descarbonizacao-do-programa-mover-explorando-variacoes-nas-vendas-de-veiculos-de-diferentes-tecnologias-ate-2027-jul24/ (accessed on 15 July 2024).
10. Instituto de Pesquisa Econômica Aplicada (IPEA). *Programa Mobilidade Verde e Inovação (Programa MOVER)*; Catálogo de Políticas Públicas, Ficha nº 995; IPEA: Brasília, Brazil, 2024. Available online: https://catalogo.ipea.gov.br/politica/995/programa-mobilidade-verde-e-inovacao-programa-mover (accessed on 27 April 2025).
11. de Oliveira Gonçalves, F.; Perna, R.F.; Lopes, E.S.; Tovar, L.P.; Filho, R.M.; Lopes, M.S. Strategies to ensure fuel security in Brazil considering a forecast of ethanol production. *Biomass* **2023**, *3*, 1–17. [CrossRef]

12. Olm, C.; Varga, T.; Valkó, É.; Hartl, S.; Hasse, C.; Turányi, T. Development of an ethanol combustion mechanism based on a hierarchical optimization approach. *Int. J. Chem. Kinet.* **2016**, *48*, 423–441. [CrossRef]
13. Hockett, A.; Hampson, G.; Marchese, A.J. Development and validation of a reduced chemical kinetic mechanism for computational fluid dynamics simulations of natural gas/diesel dual-fuel engines. *Energy Fuels* **2016**, *30*, 2414–2427. [CrossRef]
14. Kobayashi, K.; Tomioka, S.; Takahashi, M.; Kodera, M. Reaction mechanism reduction for ethylene-fueled supersonic combustion CFD. *CEAS Space J.* **2023**, *15*, 845–866. [CrossRef]
15. Saraee, H.S.; Hughes, K.J.; Pourkashanian, M. Construction of a small-sized simplified chemical kinetics model for the simulation of n-propylcyclohexane combustion properties. *Energies* **2024**, *17*, 1103. [CrossRef]
16. Marinov, N.M. A detailed chemical kinetic model for high temperature ethanol oxidation. *Int. J. Chem. Kinet.* **1999**, *31*, 183–220. [CrossRef]
17. Wang, Q.-D.; Panigrahy, S.; Yang, S.; Martinez, S.; Liang, J.; Curran, H.J. Development of Multipurpose Skeletal Core Combustion Chemical Kinetic Mechanisms. *Energy Fuels* **2021**, *35*, 6921–6927. [CrossRef]
18. Bellemans, A.; Kincaid, N.; Deak, N.; Pepiot, P.; Bisetti, F. P-DRGEP: A novel methodology for the reduction of kinetics mechanisms for plasma-assisted combustion applications. *Proc. Combust. Inst.* **2021**, *38*, 6631–6639. [CrossRef]
19. Zhu, J.; Zhou, D.; Yu, L.; Qian, Y.; Lu, X. Construction of a skeletal multi-component diesel surrogate model by integrating chemical lumping and genetic algorithm. *Fuel* **2022**, *313*, 122711. [CrossRef]
20. Shirazi, S.A.; Abdollahipoor, B.; Windom, B.; Reardon, K.F.; Foust, T.D. Effects of blending C3-C4 alcohol on motor gasoline properties and performance of spark ignition engines: A review. *Fuel Process. Technol.* **2020**, *197*, 106194. [CrossRef]
21. Silva, A.P.; Bahú, J.O.; Soccol, R., Jr.; Rodríguez-Urrego, L.; Fajardo-Moreno, W.S.; Moya, H.; León-Pulido, J.; Concha, V.O.C. Naphtha characterization (PIONA, density, distillation curve and sulfur content): An origin comparison. *Energies* **2023**, *16*, 3568. [CrossRef]
22. Li, C.; Hu, Y.; Guo, H. Study on the Simplified Chemical Kinetic Combustion Mechanism of Mixed Methanol/PODE Fuel for Marine Diesel Engines. *Processes* **2024**, *12*, 594. [CrossRef]
23. *NBR 13992*; Produtos líquidos derivados de petróleo–Determinação do teor de etanol anidro combustível (AEAC)–Método da proveta. Associação Brasileira de Normas Técnicas: Rio de Janeiro, Brasil, 2017.
24. *ASTM D4809-18*; Standard Test Method for Heat of Combustion of Liquid Hydrocarbon Fuels by Bomb Calorimeter (Precision Method). ASTM International: West Conshohocken, PA, USA, 2018.
25. *ASTM D240-17*; Standard Test Method for Heat of Combustion of Liquid Hydrocarbon Fuels by Bomb Calorimeter. ASTM International: West Conshohocken, PA, USA, 2017.
26. *ASTM D2700-19*; Standard Test Method for Research Octane Number of Spark-Ignition Engine Fuel. ASTM International: West Conshohocken, PA, USA, 2019.
27. *ASTM D2699-19*; Standard Test Method for Motor Octane Number of Spark-Ignition Engine Fuel. ASTM International: West Conshohocken, PA, USA, 2019.
28. Richards, K.J.; Senecal, P.K.; Pomraning, E. *CONVERGE 4.1*; Convergent Science: Madison, WI, USA, 2025.
29. Mittal, G.; Burke, S.M.; Davies, V.A.; Parajuli, B.; Metcalfe, W.K.; Curran, H.J. Autoignition of ethanol in a rapid compression machine. *Combust. Flame* **2014**, *161*, 1164–1171. [CrossRef]
30. Dong, S.; Wagnon, S.W.; Maffei, L.P.; Kukkadapu, G.; Nobili, A.; Mao, Q.; Pelucchi, M.; Cai, L.; Zhang, K.; Raju, M. A new detailed kinetic model for surrogate fuels: C3MechV3.3. *Appl. Energy Combust. Sci.* **2022**, *9*, 100043. [CrossRef]
31. Shi, X.; Qian, W.; Wang, Q.; Luo, H.; Kang, Y.; Ni, J. Effect of water content of hydrous ethanol on chemical kinetic characteristics based on the new developed reduced ethanol-toluene reference fuels mechanism. *Fuel* **2021**, *303*, 121201. [CrossRef]
32. Millán-Merino, A.; Fernández-Tarrazo, E.; Sánchez-Sanz, M.; Williams, F.A. A multipurpose reduced mechanism for ethanol combustion. *Combust. Flame* **2018**, *193*, 112–122. [CrossRef]
33. Zhang, L.; Qi, Q. A reduced mechanism for the combustion of gasoline-ethanol blend on advanced engine combustion modes. *Fuel* **2021**, *300*, 120951. [CrossRef]
34. Mehl, M.; Pitz, W.J.; Westbrook, C.K.; Curran, H.J. Kinetic modeling of gasoline surrogate components and mixtures under engine conditions. *Proc. Combust. Inst.* **2011**, *33*, 193–200. [CrossRef]
35. Ranzi, E.; Frassoldati, A.; Stagni, A.; Pelucchi, M.; Cuoci, A.; Faravelli, T. Reduced kinetic schemes of complex reaction systems: Fossil and biomass-derived transportation fuels. *Int. J. Chem. Kinet.* **2014**, *46*, 512–542. [CrossRef]
36. Yang, S.; Wang, Q.; Curran, H.J.; Jia, M. Development of a 5-component gasoline surrogate model using recent advancements in the detailed H2/O2/CO/C1-C3 mechanism for decoupling methodology. *Fuel* **2021**, *283*, 118793. [CrossRef]
37. Liu, Y.-D.; Jia, M.; Xie, M.-Z.; Pang, B. Development of a new skeletal chemical kinetic model of toluene reference fuel with application to gasoline surrogate fuels for computational fluid dynamics engine simulation. *Energy Fuels* **2013**, *27*, 4899–4909. [CrossRef]
38. Tsurushima, T. A new skeletal PRF kinetic model for HCCI combustion. *Proc. Combust. Inst.* **2009**, *32*, 2835–2841. [CrossRef]

39. Cota, F.S. Desenvolvimento de Mecanismos Cinéticos Químicos Reduzidos para Diferentes Misturas de Gasolina e Etanol. Master's Thesis, Universidade Federal de Minas Gerais, Belo Horizonte, Brazil, 2018.
40. Narayanaswamy, K.; Pitsch, H.; Pepiot, P. A chemical mechanism for low to high temperature oxidation of methylcyclohexane as a component of transportation fuel surrogates. *Combust. Flame* **2015**, *162*, 1193–1213. [CrossRef]
41. Ranzi, E.; Frassoldati, A.; Grana, R.; Cuoci, A.; Faravelli, T.; Kelley, A.P.; Law, C.K. Hierarchical and comparative kinetic modeling of laminar flame speeds of hydrocarbon and oxygenated fuels. *Prog. Energy Combust. Sci.* **2012**, *38*, 468–501. [CrossRef]
42. Yao, T.; Zhong, B.-J.; Luo, K.H. Compact chemical mechanism for autoignition and combustion of methylcyclohexane under engine relevant conditions. *Energy Fuels* **2017**, *31*, 11337–11347. [CrossRef]
43. Stagni, A.; Frassoldati, A.; Cuoci, A.; Faravelli, T.; Ranzi, E. Skeletal mechanism reduction through species-targeted sensitivity analysis. *Combust. Flame* **2016**, *163*, 382–393. [CrossRef]
44. Chang, Y.; Jia, M.; Li, Y.; Liu, Y.; Xie, M.; Wang, H.; Reitz, R.D. Development of a skeletal mechanism for diesel surrogate fuel by using a decoupling methodology. *Combust. Flame* **2015**, *162*, 3785–3802. [CrossRef]
45. Cai, L.; Pitsch, H. Optimized chemical mechanism for combustion of gasoline surrogate fuels. *Combust. Flame* **2015**, *162*, 1623–1637. [CrossRef]
46. Fikri, M.; Herzler, J.; Starke, R.; Schulz, C.; Roth, P.; Kalghatgi, G.T. Autoignition of gasoline surrogates mixtures at intermediate temperatures and high pressures. *Combust. Flame* **2008**, *152*, 276–281. [CrossRef]
47. Cooper, S.P.; Mathieu, O.; Schoegl, I.; Petersen, E.L. High-pressure ignition delay time measurements of a four-component gasoline surrogate and its high-level blends with ethanol and methyl acetate. *Fuel* **2020**, *275*, 118016. [CrossRef]
48. Cancino, L.R. Desenvolvimento e Aplicação de Modelos Cinéticos Detalhados para Etanol e Combustíveis Hidrocarbonetos Contendo Etanol. Ph.D. Thesis, Universidade Federal de Santa Catarina, Centro Tecnológico, Florianópolis, Florianópolis, Brazil, 2013.
49. Zhu, Z.; Liang, K.; Chen, X.; Meng, Z.; He, W.; Song, H. Laminar flame characteristics of premixed methanol–water–air mixture. *Energies* **2020**, *13*, 6504. [CrossRef]
50. Smith, G.P.; Golden, D.M.; Frenklach, M.; Moriarty, N.W.; Eiteneer, B.; Goldenberg, M.; Bowman, C.T.; Hanson, R.K.; Song, S.; Gardiner, W.C.; et al. GRI-Mech 3.0; 1999. Available online: http://www.me.berkeley.edu/gri_mech/ (accessed on 15 May 2024).
51. Pandey, H.M.; Chaudhary, A.; Mehrotra, D. A comparative review of approaches to prevent premature convergence in GA. *Appl. Soft Comput.* **2014**, *24*, 1047–1077. [CrossRef]
52. Žegklitz, J.; Pošík, P. Model selection and overfitting in genetic programming: Empirical study. In *Companion Publication of the 2015 Annual Conference on Genetic and Evolutionary Computation*; Association for Computing Machinery: New York, NY, USA, 2015; pp. 1527–1528.

Disclaimer/Publisher's Note: The statements, opinions and data contained in all publications are solely those of the individual author(s) and contributor(s) and not of MDPI and/or the editor(s). MDPI and/or the editor(s) disclaim responsibility for any injury to people or property resulting from any ideas, methods, instructions or products referred to in the content.